2016-??-????

# Time-resolved x-ray radiography of spark ignition plasma

**Alan L. Kastengren**
X-ray Science Division, Argonne National Laboratory, Illinois

**Daniel J. Duke, Andrew B. Swantek, James M. Sevik, Katarzyna E. Matusik, Thomas Wallner, Christopher F. Powell**
Energy Systems Division, Argonne National Laboratory, Illinois



**Abstract**

Understanding the short-lived structure of the plasma that forms between the electrodes of a spark plug is crucial to the development of improved ignition models for SI engines. However, measuring the amount of energy deposited in the gas directly and non-intrusively is difficult, due to the short time scales and small length scales involved. The breakdown of the spark gap occurs at nanosecond time scales, followed by an arc phase lasting a few microseconds. Finally, a glow discharge phase occurs over several milliseconds. It is during the arc and glow discharge phases that most of the heat transfer from the plasma to the electrodes and combustion gases occurs. Light emission can be used to measure an average temperature, but micron spatial resolution is required to make localized measurements. In this paper, we present the results of a proof of concept experiment that demonstrates the use of time-resolved x-ray radiography to measure the density of the plasma in the spark gap during the glow discharge phase of a conventional transistorized coil ignition system. A focused monochromatic x-ray beam from the 7-BM beamline of the Advanced Photon Source at Argonne National Laboratory was used to make time-resolved point measurements of the projected density, which decreases as the plasma temperature increases. Multiple measurement positions were combined to produce a two-dimensional map of the projected density both inside and surrounding the spark gap. A temporal resolution of 153 ns and spatial resolution of 5 $\mu$m were achieved. A range of ambient gases, densities (1 - 3 bar) and ignition coil charging durations (1 - 2.5 ms) were considered. At least 30 repeated measurements were made for each sample point and condition. All these parameters were found to substantially alter the structure of the plasma as measured by x-ray radiography. From the projected density measurements, changes in thermal energy can be calculated. These provide a quantitative measurement of the energy deposited into the gas; this is only a small fraction of the total spark energy. The measurements demonstrate the feasibility of time-resolved x-ray radiography for the study of plasma structure and development for SI applications.

## Introduction

The importance of spark plug design and operation on SI engine performance is well understood [1, 2]. Models for spark discharge have remained relatively unchanged for the last 35 years [3]. The minimum ignition energy and engine performance are understood to be a function of the mode of operation of the spark plug (arc, glow discharge, plasma jet, etc). Ultimately, this is due to changes in the method and nature of energy transfer to the gas surrounding the electrode gap [4–6].

Our present understanding of the spark discharge energy transfer process is based on the conceptual model of Maly and Vogel [3, 7]. A thorough theoretical review is given by Heywood [2]. In brief, the transfer of energy stored in the ignition coil through the spark gap begins with breakdown of the spark gap on nanosecond time scales, followed by the establishment of the arc phase which lasts on the order of a

microsecond. After the arc, a glow discharge phase of several milliseconds occurs. According to Maly and Vogel, the bulk of the heat transfer to the surrounding gas (90% or more) occurs during the glow discharge phase, during which heat transfer to the electrodes is non-negligible [3].

One of the major limitations of making experimental measurements of the evolution of the plasma in the spark gap is the very short time scales at which these phenomena occur. The fundamental physics behind spark gap breakdown are well-established [8], but the practical modeling of spark discharge for internal combustion is a complex matter that is the subject of ongoing research. More recent work on the development of 1D [9] and 2D spark discharge models [10] have coupled electrical and chemical processes to expand our understanding of the methods by which heat transfer to the surrouding gas occurs [11, 12]. To improve confidence, these simulations ultimately require empirical verification, particularly since the trends of ambient gas density, gas composition and input energy can be difficult to replicate across studies.

Experimental measurements of spark development have been undertaken for many decades, beginning with comparisons of coil current and voltage to spectroscopy of the emission from the arc [13]. Modern high-speed electronics now allow us to make detailed time-resolved measurements of the coil voltage and current, and thus the input energy profile [14]. However, there is still a need for direct non-intrusive measurements of the plasma with similarly fine temporal resolution.

High speed schlieren [15, 16] and shadowgraph imaging [17] have been successfully employed to measure the expansion radius and velocity of the kernel. However, these measurements do not provide a quantitative indication of the temperature, density, or internal energy of the plasma. Calorimetry has been used for some time to measure the evolution of the mean plasma temperature [18]. Spectrographic techniques provide useful information about the temperature, by indirectly measuring the rotational temperature of OH, vibrational temperature of $N_2$ [19] and electronic temperature [20]. Spectrography provides a useful measurement of the temperature and state of the plasma. However, the density profile is poorly understood.

Time-resolved x-ray radiography has been used for many years to make quantitative density measurements in optically dense high-speed flows [21]. In particular, high-flux synchrotron x-rays have been used to make detailed measurements of the density of high pressure diesel fuel sprays [22, 23] and cavitating fluid flows [24, 25]. Radiography can also be applied

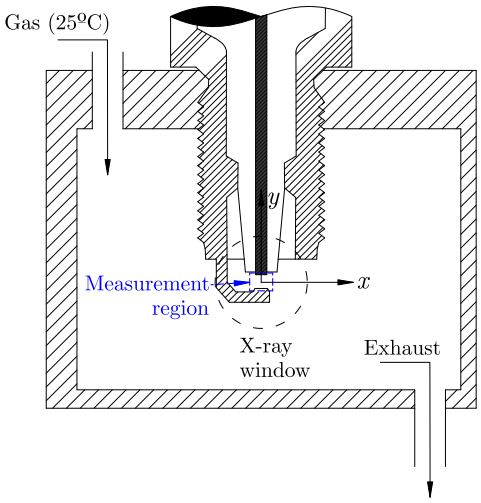


Figure 1: Cross-section of spark plug test chamber, showing co-ordinate system, measurement region and gas flow path. The x-ray beam is travelling out of the page.

to the study of plasma kernel density in a spark gap. X-rays are unaffected by temperature and pressure gradients, and scatter only very weakly [21]. Another advantage is that the measurement is unaffected by light emission from the arc, as the emission occurs at much longer wavelengths than the diagnostic [26] (the x-rays used in these experiments had a wavelength of approximately 0.2 nm).

In this paper, we present a series of proof-of-concept time-resolved measurements of gas density in the spark gap of a conventional spark plug driven by a transistorized coil. From these measurements, we can determine the total displaced volume and change in enthalpy of the plasma during the transition and glow discharge phases, where most of the heat transfer to the surrounding gas occurs. Measurements have been made in both air and argon at various densities and coil charging durations.

**Method**

In order to study the spark kernel development in a controlled environment, a spark plug was placed in a grounded, enclosed chamber through which a continuous stream of gas flowed. The spark plug was oriented as shown in Fig. 1, with the measurement region centered on the 1mm gap between the electrode and ground (the x-ray beam is traveling out of the page). Experiments were conducted in both air and argon at several densities. The chamber was fitted with a pair of polyimide windows to allow the x-ray beam to pass through the measurement region while the chamber was pressurized. The spark plug was operated by a conventional transistorized coil driver

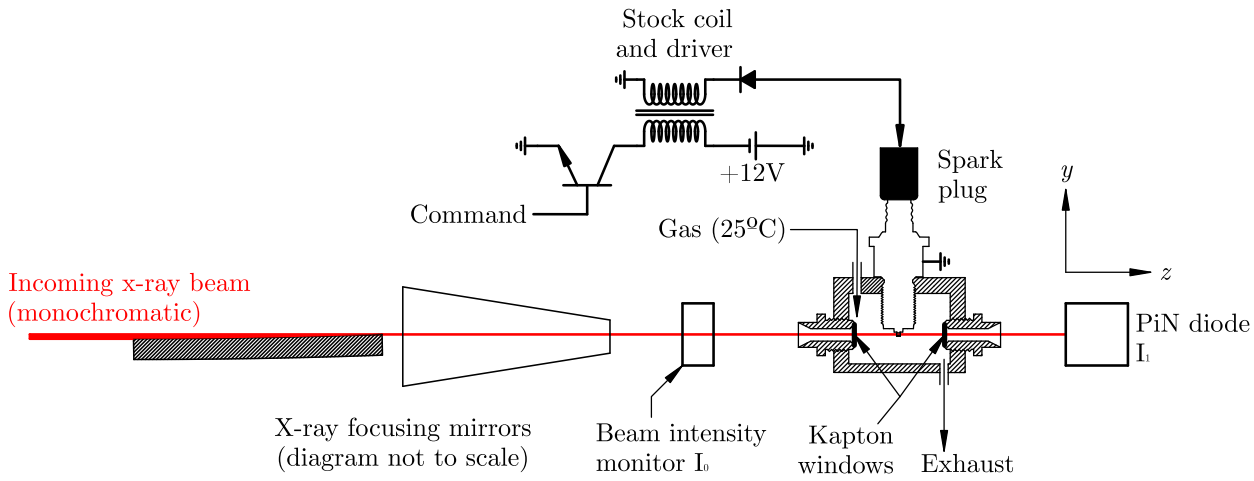


Figure 2: Schematic diagram of beamline and experiment setup (not to scale). The monochromatic x-ray beam (red line) travels left to right. The electrical circuit is a simplified representation of the key components of the stock coil and transistorized driver, which was externally triggered.

(Fig. 2). Several charging times were tested, up to the saturation limit of the coil. The stored energy in the coil was determined by measuring the current supplied during the charging phase and integrating over time - see Table 1. The uncertainties represent 2 standard deviations of the stored energies.

X-ray radiography measurements were performed at the 7-BM beamline of the Advanced Photon Source at Argonne National Laboratory [27]. In this experiment, we used a monochromatic x-ray beam of mean energy 6 keV, 4.2% full width at half maximum energy bandpass. The beam was focused to a spot approximately $5 \times 6$ $\mu$m using a pair of x-ray mirrors (Fig. 2). The beam focus was aligned with the spark gap; the divergence was small compared to the measurement region. The beam intensity was monitored upstream of the experiment ($I_0$), and the transmitted beam ($I$) was measured with a PIN diode. The chamber was traversed through the fixed beam in order to build up a raster-scan pattern of measurements, as shown in Fig. 3.

The transmission of monochromatic x-rays along the line of sight of the beam may be related to the change in density of the material in the beam path with time

| Coil charging time | Stored energy |
|---|---|
| 1.0 ms | $14.89 \pm 3.07$ mJ |
| 1.5 ms | $29.77 \pm 2.83$ mJ |
| 2.0 ms | $48.73 \pm 5.02$ mJ |
| 2.5 ms | $71.53 \pm 2.77$ mJ |

Table 1: Stored energy in the coil as measured by the time-integral of the current delivered to the primary winding at 12V DC.

via the Lambert-Beer law;

$$\Delta M(x,y,t) = \int \rho(x,y,z,t) - \rho_0 dz = \frac{-1}{\mu} \ln\left(\frac{I(x,y,t)/I(x,y,0)}{I_0(x,y,t)/I_0(x,y,0)}\right). \quad (1)$$

Here, the transmission $I(x,y,t)$ is normalized by both the incoming beam intensity $I_0$ and the initial intensity $I(x,y,0)$ to yield a change in projected mass $\Delta M(x,y,t)$ (units mass per area) which is calibrated by the attenuation coefficient $\mu$. The attenuation coefficient is a well-known function of the gas composition and x-ray energy and is obtained from lookup tables [28]. If the ambient gas density $\rho_0$ is known *a priori*, then the change in projected mass in the beam path can be converted to an equivalent pathlength, which represents the volume displacement of ambient gas by the plasma integrated over the beam area;

$$L(x,y,t) = \Delta M(x,y,t)/\rho_0. \quad (2)$$

Furthermore, we can compute the total displaced volume of ambient gas due to the plasma by integrating over the measurement area;

$$\Delta \forall\,(t) = \iint L(x,y,t)\, dx\, dy. \quad (3)$$

This calculation assumes that the entire plasma is contained within the measurement region. If an ideal gas assumption is made, it is then relatively straightforward to compute the increase in the enthalpy of the gas due to thermal expansion at constant pressure by integrating over the measurement domain;

$$\Delta H(t) = \Delta \forall\,(t)\, \rho_0 C_p T. \quad (4)$$

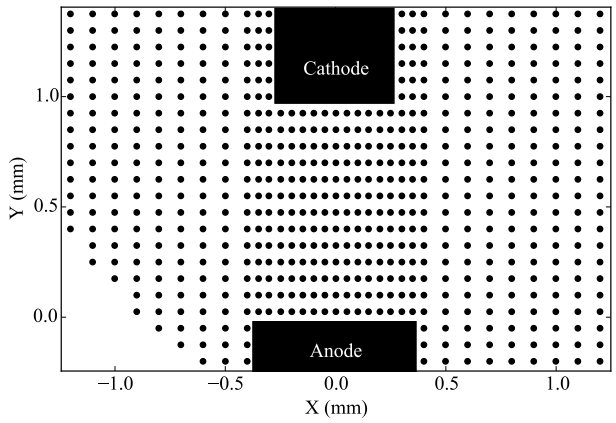


Figure 3: Measurement grid for the radiography data, shown relative to the electrode positions.

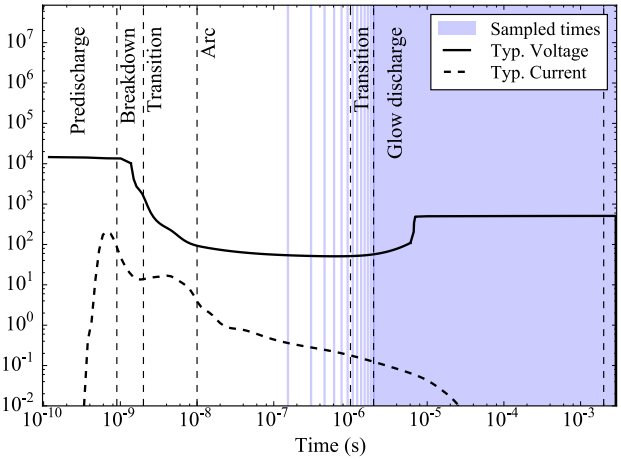


Figure 4: Timing diagram, showing nominal voltage and current profiles for a spark plug to nearest order of magnitude, adapted from the conceptual model of Maly and Vogel [2, 3]. The blue regions show times that are sampled by x-ray radiography.

The incident x-ray beam is not continuous, but consists of a series of pulses. In these experiments, a series of 24 equally-spaced pulses (33.5 ps mean duration, 153 ns apart) were used. The resulting measurement bandwidth is represented in the timing diagram of Fig. 4. The conceptual voltage and current curves based on the model of Maly and Vogel [3] are shown on a log-log scale. The blue region indicates regions in the time domain that were able to be measured. Several sample points were captured during the arc phase, but the temporal resolution here is too coarse to be able to properly capture the initial shockwave. However, the bandwidth is sufficient to properly capture the transition and glow discharge phases.

**Results**

The measurements reveal that the structure of the plasma varies greatly depending on the gas composition and ambient density. Several series of two-dimensional plots of equivalent gas pathlength (Eqn. 2) are shown in Figures 5-7.

In Fig. 5, we show six time snapshots for a spark with 2.5 ms charging time in a 1 bar ambient argon environment. In fig. 5a, 6 $\mu$s after the command signal, the arc has not yet occurred. In Fig. 5b, 13 $\mu$s after command, the arc phase is already complete and the transition to glow discharge is in progress. We see a growing region of low density (negative pathlength) occuring in a cylindrical region between the electrodes, with the lowest density values near the cathode (upper part of the image). In figs. 5c-d, 32 to 57 $\mu$s after command, the local density continues to fall and the lowest density region remains close to the cathode. This is the region in which electrons are deposited into the gas and ionisation is expected to be strongest. By 200 $\mu$s (fig. 5e), the low-density region near the cathode has disappeared and the density profile is approximately symmetric between the electrodes. While the radial profile is not directly observed due to the line-of-sight nature of the measurement, the profiles appear very symmetric from left to right (around the vertical axis between the electrodes). At 1.37ms after command (fig. 5f), the gas pathlength reaches its lowest value, and the displacement of the gas takes on an oblate spheroid shape. After this point, the system relaxes to equilibrium over tens of milliseconds.

In Fig. 6, we can see the effect of increasing the ambient pressure from 1 bar to 3 bar. Again, the low density first appears near the cathode in Fig. 6b. However, the low density region develops more slowly and remains concentrated in a region near the cathode and does not appear axisymmetric (Figs. 6c-d). After approximately 1ms, the density reaches its minimum and relaxes back to ambient (Figs. 6e-f).

If we now change the gas from argon to air (Fig. 7), while keeping the ambient pressure constant at 3 bar, we again see a very large change in the spatial density distribution. In Fig. 7a, we see evidence over the first 20 $\mu$s of the shock wave generated by the arc, as a high-density region travels outward from the space between the electrodes. In Fig. 7b, we see the formation of a large low-density region which grows from the space between the electrodes, rather than from the cathode, as was the case for the argon measurements. Rather than expanding equally in all directions, this low density region expands faster in the horizontal than the vertical (Figs. 7c-e). After the minimum value is reached (Fig. 7e), the low density takes much longer to relax to equilibrium than for the argon cases.

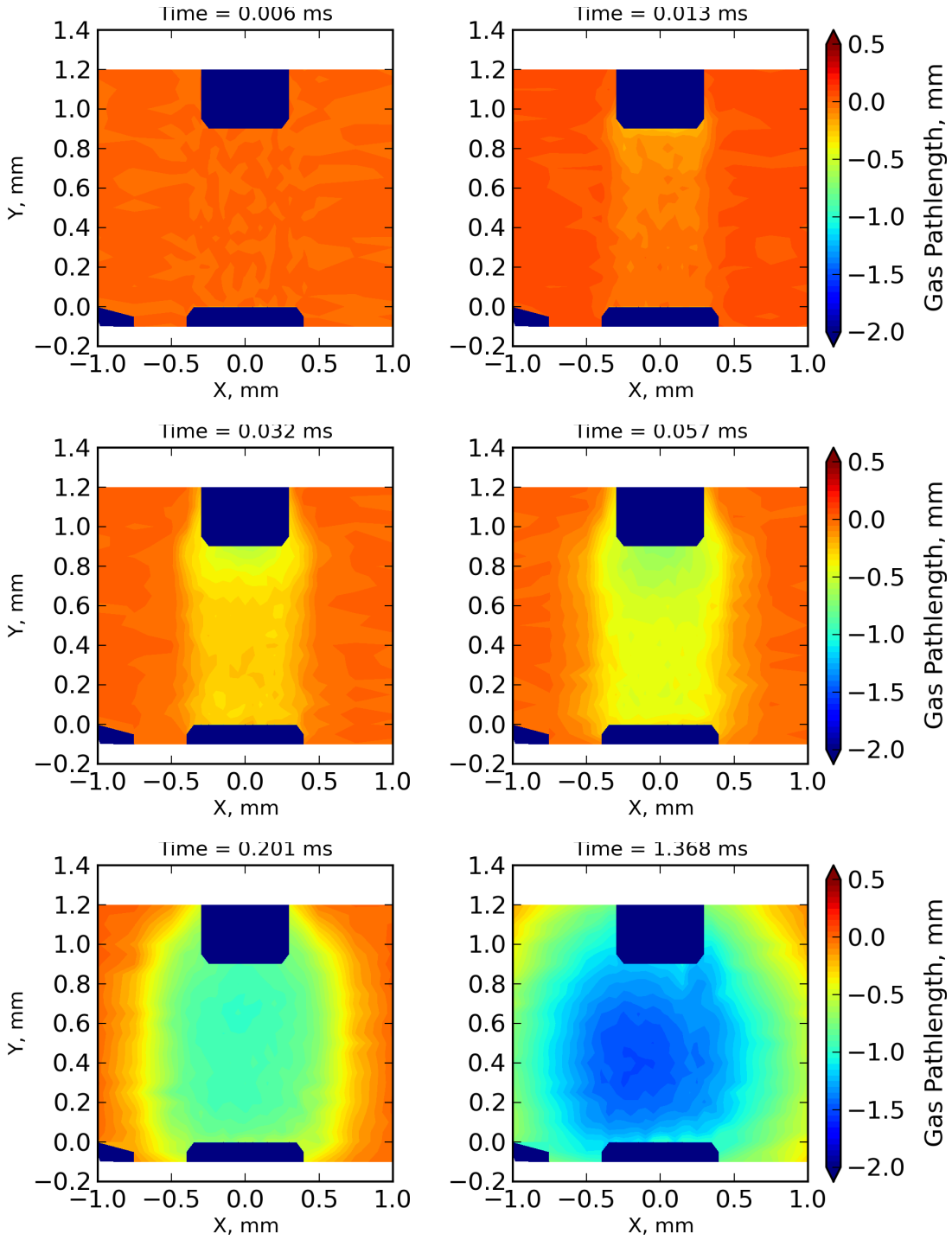


Figure 5: Time evolution of the gas displacement for 2.5ms charge time in a 1 bar Ar ambient environment. The center electrode is at the top of the image.

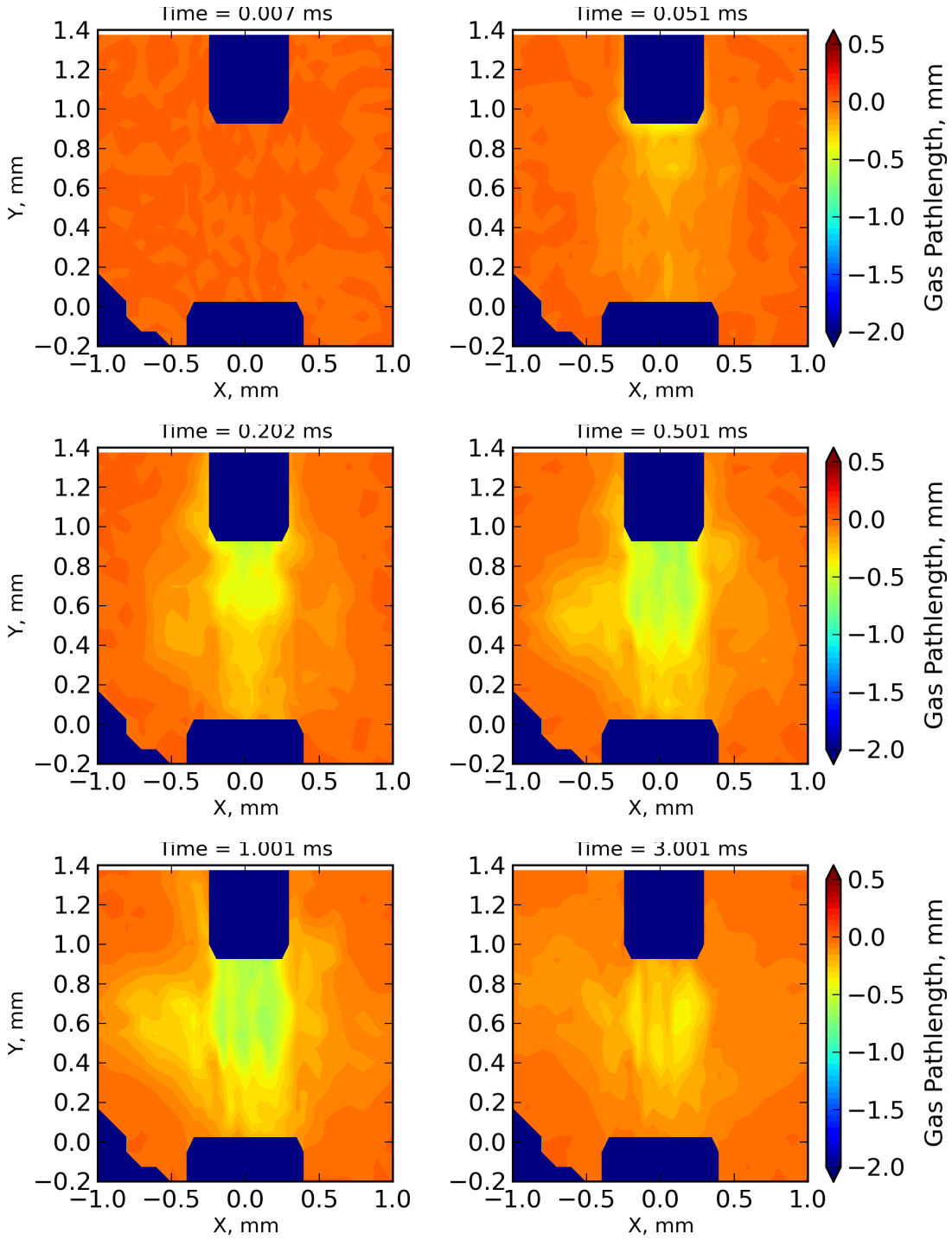


Figure 6: Time evolution of the gas displacement for 2.5ms charge time in a 3 bar Ar ambient environment. The center electrode is at the top of the image.

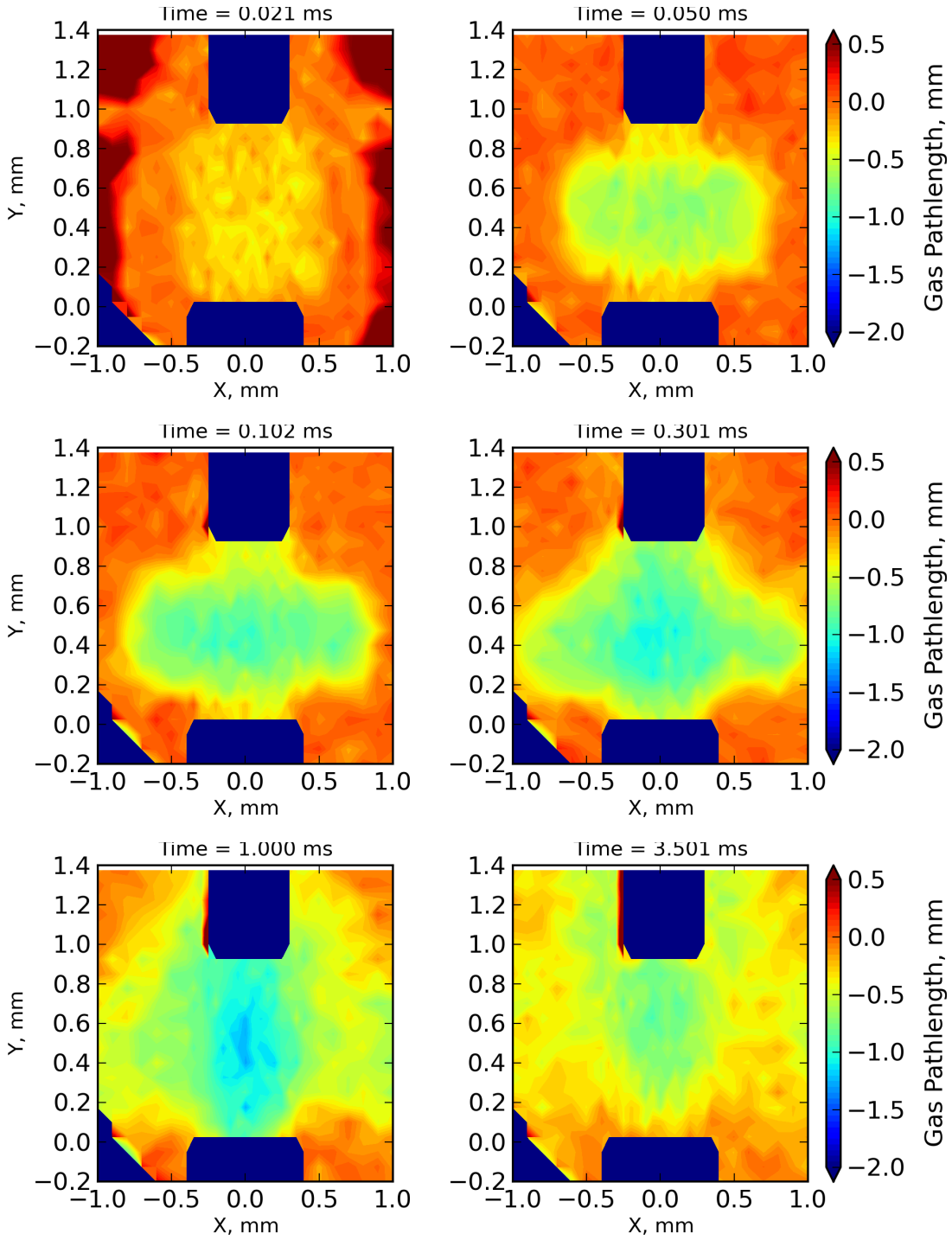


Figure 7: Time evolution of the gas displacement for 2.5ms charge time in a 3 bar air ambient environment. The center electrode is at the top of the image.

The measurements of effective pathlength deficit in the plasma can be used to estimate the local density by assuming an elliptical profile about the $y$ axis . If we consider the measurement domain in cylindrical co-ordinates, and assume that the plasma density is uniform over an elliptic cross-section in the $x-z$ plane, the projection of this density field in $z$ can be fitted to the radiography measurements (Eqn. 1) using a least-squares approach. We solve an elliptical distribution for the fitting coefficients $a$,$b$ and the effective elliptical profile density $\rho_e$, which are functions of $y$ and time;

$$M(x,y,t) = 2\rho_e(y,t)\sqrt{1-\left(\frac{x-a(y,t)}{b(y,t)}\right)^2}. \quad (5)$$

Once $\rho_e$ is estimated, a fractional density deficit function can be calculated, representing the fraction decrease in ambient density;

$$\mathrm{DD}(y,t) = \frac{\rho_0 - \rho_e(y,t)}{\rho_0}. \quad (6)$$

The results are plotted in Fig. 8. Here, the density deficit (dimensionless) is shown against the vertical distance $y$ between the electrodes (vertical axis) and time (horizontal axis) along the centerline ($x = 0$).

The results for two of the four measured charging durations in 4 bar ambient are are shown. We firstly note the appearance of a sudden, uniform low density between the electrodes at a very distinct moment in time, rather than a gradual decrease of density from the cathode downwards. Following this rapid transient, the density remains lower in the center and returns to a near-equilibrium value at the electrodes. The faster recovery of density near the electrodes may be explained by heat transfer into the metal. After about 100 $\mu$s, the distribution again becomes more uniform. At the end of the glow discharge, the density field returns to equilibrium, starting near the electrodes and ending at the center. Again, the faster recovery near the electrodes may be explained by heat transfer.

In Fig. 9, we compare the total volume displacement (Eqn. 3, left vertical axis) and thermal energy (Eqn. 3, right vertical axis) against time (horizontal axis) for all the measured conditions. The most striking comparison between the argon experiments (figs. 9a-b) and air experiments (figs. 9c-d) are that the spark in air has a very strong transient discontinuity approximately 10 $\mu$s after command. The discontinuity in the argon measurements is much smaller. We propose that this discontinuity is due to the shock wave generated by the arc (Fig. 7a). The second feature of note is the presence of oscillations in displacement and energy from approximately 30 to 300 $\mu$s after command. These oscillations are much stronger for the air experiments than the argon. Noting that the sound speed and compressibility of air and argon are very similar at 300K, we hypothesise that the shock wave and oscillation differences may be related to the difference in breakdown voltage; the Paschen breakdown voltage for air is approximately seven times higher than that of argon for the relevant pressure range [29], and as such the breakdown will occur with more stored energy in the gap (greater capacitance). The timing of the peak thermal energy is also given for each condition in Fig. 9; this will be discussed later.

In Fig. 10, we show the secondary coil voltage and primary coil current traces for all the measured conditions. The origin of the time axis is defined as the moment at which breakdown occurs. Since the current (dashed line) is only measured on the primary side, it is zero for $t > 0$. We note firstly that a negative voltage is induced in the coil during charging ($t < 0$). At $t \approx 0$, breakdown is indicated by a rapid drop in the voltage induced by the secondary. This is followed by a gradual increase, peak and decrease of the secondary voltage during the glow discharge. An important feature of note in the voltage profile is the presence of a kink or oscillation at $t \approx 1$ ms, denoted by the arrows in Fig. 10. We propose that this is due to the quenching of the arc. In the argon data, this is followed by a rapid increase in gap voltage (due to higher impedance). In Fig. 11, we compare the time delay between breakdown and quench (denoted as arc duration) from the voltage probe data over all the measured conditions. We note that the duration is strongly correlated with charging time and somewhat dependent on gas composition, but there is no clear trend with ambient density. It is strongly correlated with delay time for the peak density deficit shown in Fig. 9, but not equal to it. In the present setup, we were unable to record the secondary coil current; in future work this will provide confirmation of the arc duration.

We have also compared the timing and magnitude of the peak thermal energy and volume displacement from the data in fig. 9. This peak typically arrives about 1 ms after command. The gap then takes tens of milliseconds to return to equilibrium. Fig. 12 shows the dependence of the timing of this peak (left plot) and the magnitude of the peak (right plot) as a function of the charging time (horizontal axis) and the ambient density (color scale). We note that the delay to the peak is strongly correlated with the charging time, and only weakly correlated with the ambient density. This is intutitive, since the minimum impedance of the gap during the glow discharge will limit the current,

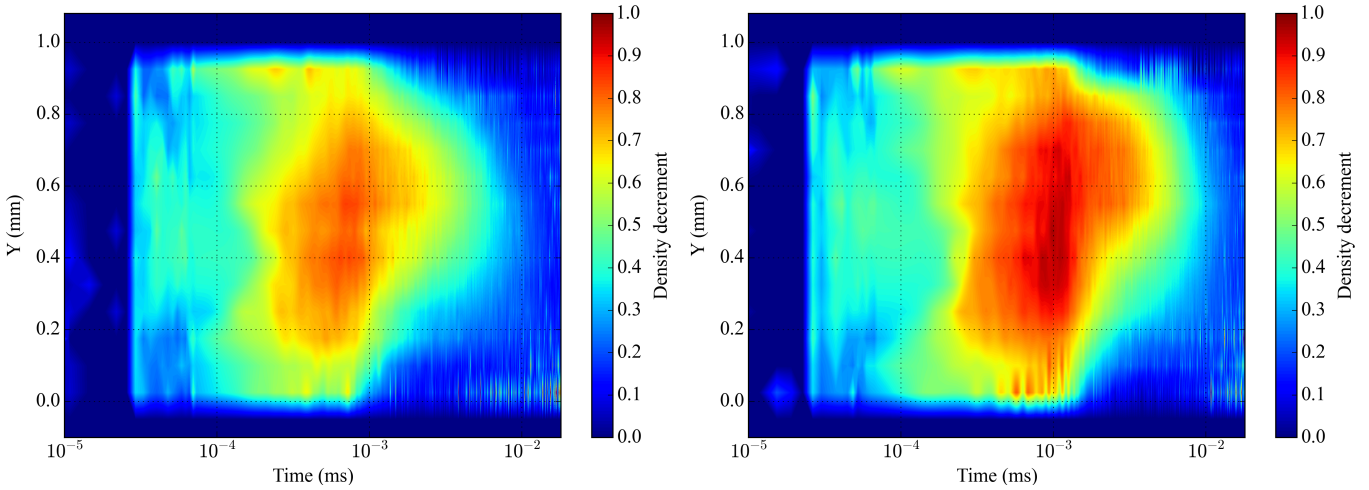


(a)4 bar air ambient, 1.0 ms charging time.

(b)4 bar air ambient, 1.5 ms charging time.

(c)4 bar air ambient, 2.0 ms charging time.

(d)4 bar air ambient, 2.5 ms charging time.

Figure 8: Fractional decrement in density, determined by elliptic fitting in the $x$ (transverse) axis. The horizontal axis is time, and the vertical axis is the distance between the electrodes. The time scales shown here range from 10 $\mu$s after the commanded spark trigger to 20 ms.

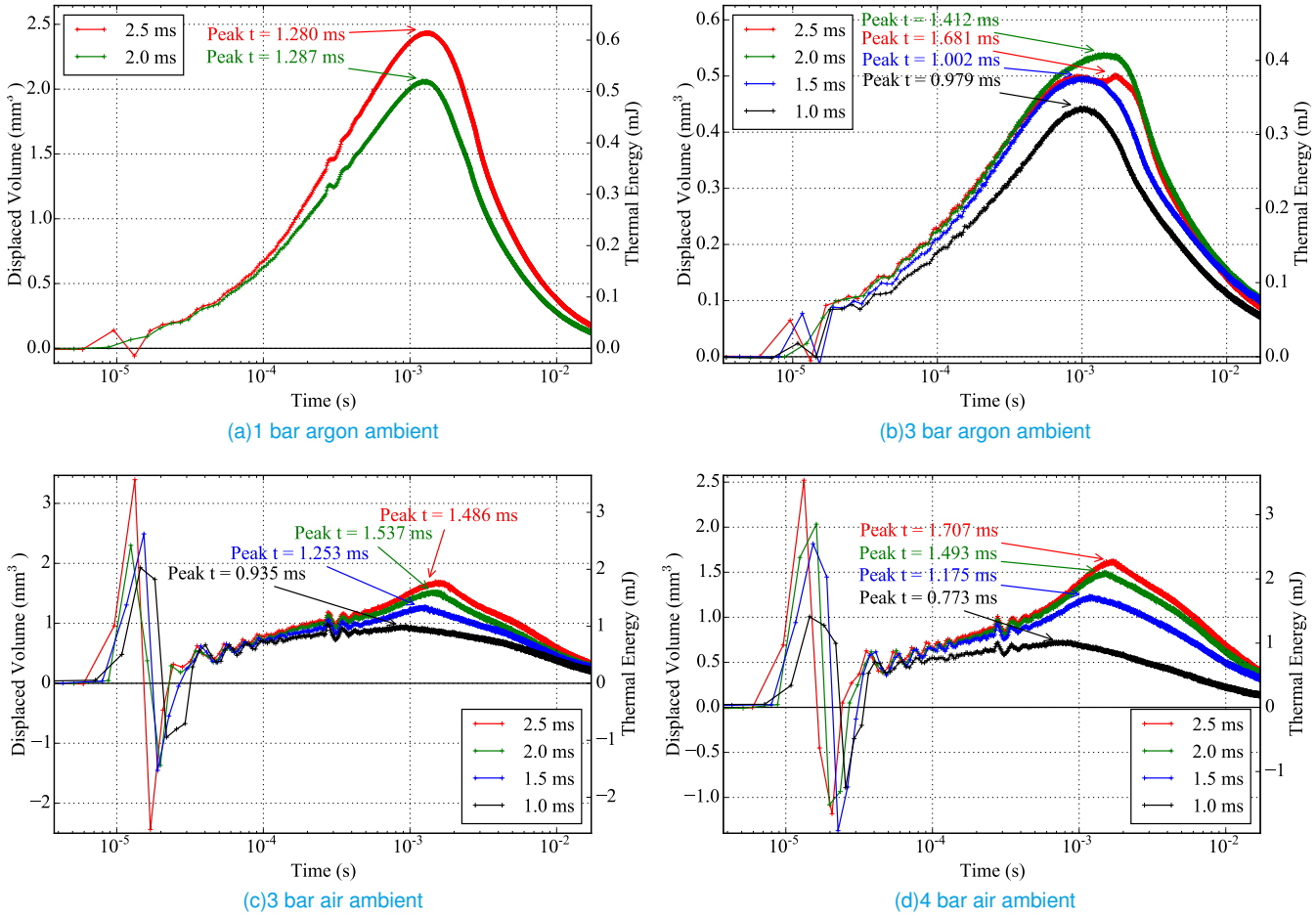


Figure 9: Spatially integrated volume displacement and thermal energy as a function of time for argon (a-b) and air (c-d) for several charging times (varying colors).

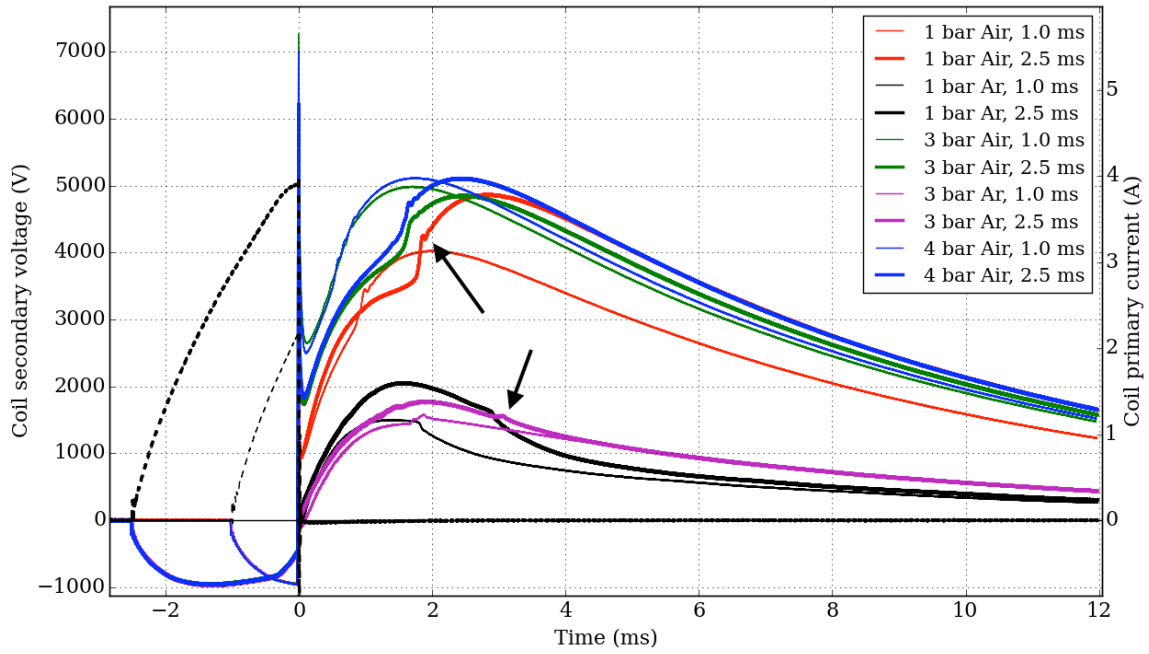


Figure 10: Secondary coil voltage (solid lines, left vertical axis) and primary coil current (dashed lines, right vertical axis) shown as a function of time relative to breakdown (horizontal axis) for all measured conditions. The line color indicates the gas composition and ambient pressure, and the line thickness indicates the coil charging time (as per legend).

and as the total energy input increases, the timescales will increase correspondingly. However, the peak displacement and arc duration times (Figs. 11-12) are not strongly correlated. According to the established model, we expect a decreasing current flow throughout the glow discharge [3]. As such, the peak thermal energy may depend on the changing balance between heat loss to the ambient and addition from ohmic heating, which operate on independent timescales.

We also note that the time delay to peak secondary voltage during the glow discharge phase (Fig. 10) do not correlate strongly, but occur at different times (up to 0.5 ms earlier or later). We also find that the magnitude of the peak is strongly dependent on the ambient density and composition, and only moderately dependent on the charging time. This suggests that the degree of density deficit depends on the properties of the gas. Once again, if the current is limited as charging time increases, then ohmic heating of the gas will not increase substantially.

**Conclusions**

In this paper, we have presented the first x-ray radiography measurements of plasma evolution in a conventional spark plug gap. These proof of concept measurements demonstrate some of the effects of gas composition, density, and charging time on the structure of the plasma. From the radiography measurements, we calculated the displaced pathlength of ambient gas, the total integrated volume displacement of ambient gas, and the approximate change in thermal energy. By making an elliptical least-squares fit in the horizontal plane, we were also able to calculate the decrement of density as a function of vertical electrode distance and time.

We find that the spatial structure of the plasma varies greatly between argon and air, suggesting that the ionisation potential of the gas may be an important factor. In argon, we find that the low density region grows downward from the cathode to the anode, while in air, the low density region appears to grow uniformly in the vertical direction. The initial arc shock wave and following high-frequency oscillations also vary noticeably between the two different ambient gases. All the experiments show a peak in thermal energy and volume displacement approximately 1 ms after command, and relax back to equilibrium after tens of milliseconds.

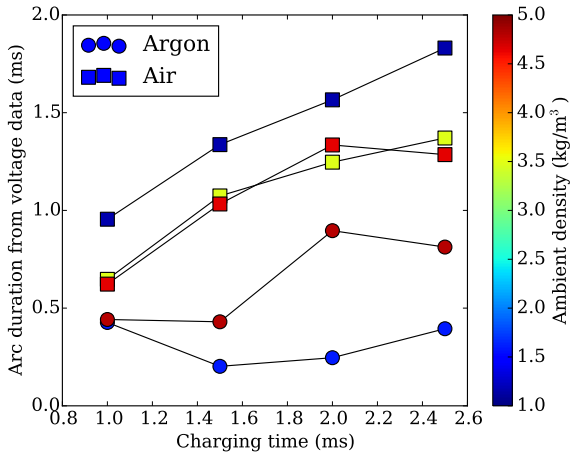


Figure 11: Delay between breakdown and arc quench as indicated by the secondary coil voltage (see Fig. 10) as a function of charging time (horizontal axis), gas composition and ambient density (color).

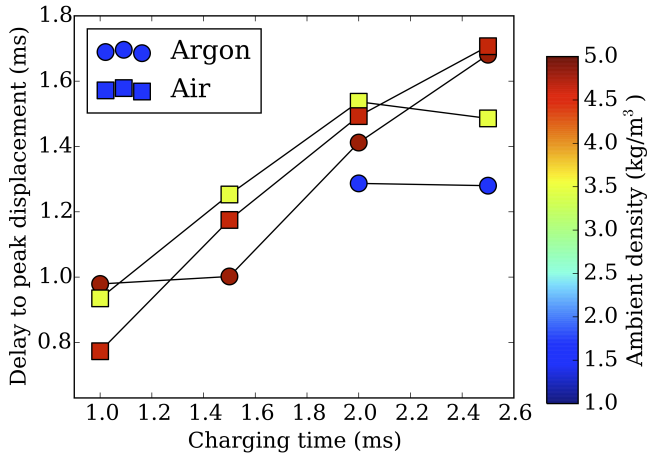


(a) Delay time to peak thermal energy.

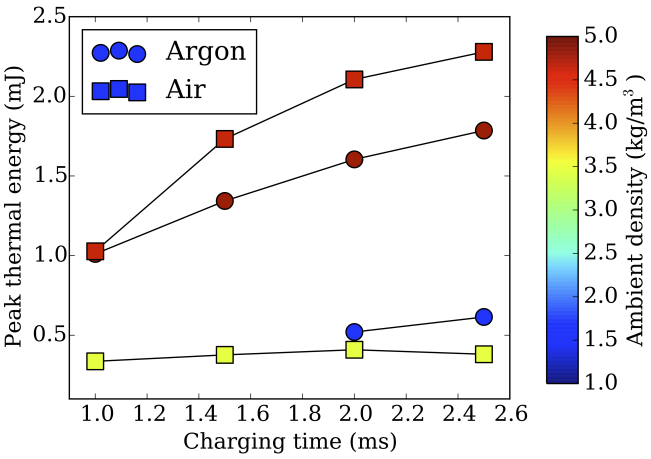


(b) Peak magnitude of thermal energy.

Figure 12: Delay (a) and magnitude (b) of the peak thermal energy from x-ray radiography as a function of charging time (horizontal axis), gas composition and ambient density (color).

Analysis of the intensity and timing of the peak volume displacement and thermal energy suggest that the peak delay is strongly dependent on the charging time, and only weakly on the ambient density. This suggests that the current flow may be a controlling factor. The intensity of the peak displacement and thermal energy is strongly dependent on the ambient density and composition, and moderately on the charging time. This suggests again that the properties of the gas play an equally important role as the amount and rate of energy deposited. The secondary coil voltage and spark gap energy evolve over slightly different time scales, suggesting that effects other than the current flow and voltage across the gap (such as the density and structure of the plasma) need to be considered.

In future work, we will refine these proof of concept measurements by comparing time-resolved gap voltage and coil current to the x-ray measurements, and investigating a wider range of operating conditions. The effect of spark plug design will also be investigated. In this study, multiple measurements were taken to compute an ensemble average. In future work, repeatability will be investigated by considering single-event statistics. X-ray radiography measurements provide useful information which may be combined with established diagnostics (spectroscopy, calorimetry, imaging, etc.) to provide more complete validation methods for ignition modeling, and improve our fundamental understanding of spark plug operation.

**Acknowledgments**

The authors wish to thank Dr. Michael Czekala (Ford) for helpful discussions during the preparation of this paper. This research was performed at the 7-BM beam line of the APS at Argonne National Laboratory. Use of the APS is supported by the U.S. Department of Energy (DOE) under Contract No. DE-AC02-06CH11357. This work is an extension of Argonne's fuel spray research, sponsored by the DOE Vehicle Technologies Program under the direction of Gurpreet Singh and Leo Breton.

**References**

[1] R R Burgett, J M Leptich, and K V S Sangwan. Measuring the Effect of Spark Plug and Ignition System Design on Engine Performance. SAE transactions, 81(1):48–67, January 1972.

[2] J B Heywood. Internal Combustion Engine Fundamentals. McGraw-Hill, January 1988.

[3] R Maly and M Vogel. Initiation and propagation of flame fronts in lean CH 4-air mixtures by the three modes of the ignition spark. In Proc. Symposium (International) on Combustion, pages 821–831, 1979.

[4] D R Ballal and A H Lefebvre. The influence of flow parameters on minimum ignition energy and quenching distance. In Proc. Symposium (International) on Combustion, pages 1473–1481, 1975.

[5] D R Ballal and A H Lefebvre. The influence of spark discharge characteristics on minimum ignition energy in flowing gases. Combustion and Flame, 24:99–108, 1975.

[6] GFW Ziegler, E P Wagner, and R R Maly. Ignition of lean methane-air mixtures by high pressure glow and arc discharges. In Proc. Symposium (International) on Combustion, pages 1817–1824, 1985.

[7] R Maly. Ignition model for spark discharges and the early phase of flame front growth. In Proc. Symposium (International) on Combustion, pages 1747–1754, 1981.

[8] E Sher, J Ben-Yaish, and T Kravchik. On the Birth of Spark Channels. Combustion and Flame, 89:186–194, January 1992.

[9] M Schäfer, R Schmidt, and J Köhler. 1-d simulation of a spark discharge in air. In Proceedings of the Combustion Institute, pages 2701–2708, January 1996.

[10] M Thiele, S Selle, U Riedel, J Warnatz, and U Maas. Numerical Simulation of Spark Ignition Including Ionization. In Proceedings of the Combustion Institute, pages 1177–1185, March 2000.

[11] O Yasar. A new ignition model for spark-ignited engine simulations. Parallel Computing, 27:179–200, February 2001.

[12] O Ekici, O A Ezekoye, M J Hall, and R D Matthews. Thermal and Flow Fields Modeling of Fast Spark Discharges in Air. Journal of Fluids Engineering, 129(1):55–11, 2007.

[13] H Albrecht, W H Bloss, W Herden, R Maly, B Saggau, and E Wagner. New Aspects on Spark Ignition. In SAE Technical Paper 770853, Detroit, MI, September 1977.

[14] M J Lee, O A Ezekoye, and R Matthews. Voltage, and Energy Deposition Characteristics of Spark Ignition Systems. In SAE Paper 2005-01-0231, 2005.

[15] S P M Bane, J L Ziegler, P A Boettcher, S A Coronel, and J E Shepherd. Experimental investigation of spark ignition energy in kerosene, hexane, and hydrogen. Journal of Loss Prevention in the Process Industries, 26(2):290–294, March 2013.

[16] Sally P M Bane, Jack L Ziegler, and Joseph E Shepherd. Investigation of the effect of electrode geometry on spark ignition. Combustion and Flame, 162(2):462–469, February 2015.

[17] D M Carmo and E C Fernandes. Analysis of Spark Discharges. In 17th International Symposium on Applications of Laser Techniques to Fluid Mechanics, Lisbon, Portugal, July 2014.

[18] Brandon Sforzo, Alexander Lambert, Jaecheol Kim, Jeff Jagoda, Suresh Menon, and Jerry Seitzman. Post discharge evolution of a spark igniter kernel. Combustion and Flame, 162(1):181–190, January 2015.

[19] B Hnatiuc, D Astanei, S Pellerin, N Cerqueira, and M Hnatiuc. Diagnostic of Plasma Produced by a Spark Plug at Atmospheric Pressure: Reduced Electric Field and Vibrational Temperature. Contributions to Plasma Physics, 54(8):712–723, March 2014.

[20] C Oliveira, J L Reis Jr, J A Souza-Corrêa, A Dal Pino Jr, and J Amorim. Optical and electrical diagnostics of a spark-plug discharge in air. Journal of Physics D: Applied Physics, 45(25):255201–8, June 2012.

[21] A Kastengren and C F Powell. Synchrotron X-ray techniques for fluid dynamics. Experiments in Fluids, 55(3):1686, February 2014.

[22] A L Kastengren, F Tilocco, D Duke, C Powell, X Zhang, and S Moon. Time-resolved x-ray radiography of sprays from engine combustion network spray a diesel injectors. Atomization and Sprays, 24(3):251–272, May 2014.

[23] A B Swantek, A L Kastengren, D J Duke, F Z Tilocco, N Sovis, and CF Powell. Quantification of Shot-to-Shot Variation in Single Hole Diesel Injectors. SAE International Journal of Fuels and Lubricants, 8(1):160–166, April 2015.

[24] D Duke, A L Kastengren, F Tilocco, A B Swantek, and CF Powell. X-ray Radiography Measurements of Cavitating Nozzle Flow. Atomization and Sprays, 23(9):841–860, October 2013.

[25] D J Duke, A B Swantek, A L Kastengren, K Fezzaa, and C Powell. Recent Developments in X-ray Diagnostics for Cavitation. SAE International Journal of Fuels and Lubricants, 8(1):135–146, April 2015.

[26] E M Bazelyan and Yu P Raizer. Spark Discharge. CRC Press, Boca Raton, 1998.

[27] A Kastengren, C F Powell, D Arms, E M Dufresne, H Gibson, and J Wang. The 7bm beamline at the aps: a facility for time-resolved fluid dynamics measurements. Journal of synchrotron radiation, 19(4):654–657, May 2012.

[28] B L Henke, E M Gullikson, and J C Davis. X-ray interactions: photoabsorption, scattering, transmission, and reflection at $E = 50 - 30000$ eV, $Z = 1 - 92$. Atomic Data and Nuclear Data Tables, 54(2):181–342, 1993.

[29] J Benyon. Conduction of Electricity Through Gases. Harrap, 1972.